PERGAMON

International Journal of Heat and Mass Transfer 44 (2001) 1201–1212

International Journal of HEAT and MASS TRANSFER

www.elsevier.com/locate/ijhmt

A statistical analysis of EHD-enhanced nucleate boiling along a heated wire

C.C. Pascual, S.M. Jeter, S.I. Abdel-Khalik *

George Woodruff School of Mechanical Engineering, Georgia Institute of Technology, Atlanta, GA 30332-0405, USA

Received 2 September 1999; received in revised form 28 April 2000

Abstract

Saturated nucleate boiling experiments of HCFC-123 along a 0.13 mm diameter platinum wire with an applied uniform electric field were conducted. High-speed video imaging was used to measure the average number density of active nucleation sites, the average bubble departure frequency per nucleation site, and the frequency distribution of bubble departure diameters. At a given heat flux, application of an electric field increases the natural convection contribution to the total heat flux, while the latent heat and forced convection contributions are reduced, due to reductions in the number of active nucleation sites and the average bubble departure diameter.

1. Introduction

Application of an electric field to a dielectric is known to enhance heat transfer. This effect is commonly known as electrohydrodynamic (EHD) enhancement; it has been known since Chubb [1] performed his experiments with water. By applying an electric field to a boiling dielectric fluid, both the vapor bubble dynamics and the liquid motion are modified. While EHD enhancement of boiling heat transfer has been extensively studied, the fundamental effect of the EHD force on bubble dynamics, and hence, the boiling process, has not been quantified. Therefore, the primary purpose of this investigation was to determine how EHD affects bubble dynamics and the contributions of various mechanisms to the boiling heat flux. The data obtained in this investigation provide the means to validate the applicability and accuracy of various mechanistic nucleate boiling models in the presence of an electric field. To achieve these objectives, an experimental investigation of the effect of EHD on bubble dynamics in saturated nucleate pool boiling of HCFC-123 from a heated wire was conducted. The effect of the electric field on the average number density of active nucleation sites, the average bubble departure frequency per nucleation site, and the frequency distribution of bubble departure diameters have been determined. These data were then used to determine the contributions of natural convection, forced convection, and latent heat transfer to the total surface heat flux following the mechanistic model of Paul and Abdel-Khalik [2]. A brief review of earlier work on EHD enhancement of boiling heat transfer is first presented.

The effect of EHD on single and two-phase heat transfer can be understood by examining the expression for the electric force density on a dielectric fluid under the influence of an electric field [3]

$$\overline{F_v} = q\bar{E} + \frac{1}{3}\varepsilon_0(\varepsilon-1)E^2\frac{\mathrm{d}\varepsilon}{\mathrm{d}T}\nabla T + \frac{1}{6}\varepsilon_0(\varepsilon-1)(\varepsilon+2)\nabla E^2. \quad (1)$$

Eq. (1) has been modified to remove the direct density dependence of the liquid dielectric constant by using the Clausius–Mossotti law [3]. The first term on the right, called electrophoresis, is due to the Coulomb force upon a charged particle in a dielectric fluid. The second term is called electroconvection and represents the force density

* Corresponding author. Tel.: +1-404-894-3719; fax: +1-404-894-3733.

E-mail address: said.abdelkhalik@me.gatech.edu (S.I. Abdel-Khalik).

0017-9310/01/$ - see front matter
PII: S0017-9310(00)00149-6

Nomenclature

C_1, C_2	constants in Eq. (17)
D_w	platinum wire diameter (m)
$\langle D \rangle$	average bubble departure diameter (m)
E	electric field strength (V/m or N/C)
El	electrical number: $(El = \rho(d\varepsilon/dT)D_w^2 \Delta T \varepsilon_0 E^2)/\mu^2$ (properties evaluated at film temperature)
$\langle F \rangle$	average bubble departure frequency (s^{-1})
F_v	electric force density (N/m^3)
f	fraction of surface experiencing either latent heat transfer, natural convection, or forced convection
f_1	fractional number of bubble diameters beyond the perimeter of the bubble which experiences agitation
f_g	average fractional chord length of a spherical bubble in contact with surface
g	gravitational acceleration (m/s^2)
h	heat transfer coefficient (W/m^2 K)
h_{fg}	enthalpy of vaporization (J/kg)
I	current (A)
$\langle J \rangle$	average heat removal per bubble (J)
k	thermal conductivity (W/m K)
L	length of platinum wire (m)
$\langle N \rangle$	average number of nucleation sites per unit length (l/m)
Nu	Nusselt number: $Nu = (hD_w)/k$ (properties evaluated at film temperature)
$\langle Nu \rangle$	average Nusselt number
n	constant used in Eq. (10) given by Eq. (11)
Pr	Prandtl number: $Pr = v/\alpha$ (properties evaluated at film temperature)
q	free charge density (C/m^3)
q''	heat flux (W/cm^2)
Ra	Rayleigh number: $Ra = (g\beta(T_S - T_\infty)D_w^3)/v\alpha$ (properties evaluated at film temperature)
Ra_{El}	electric Rayleigh number: $Ra_{El} = El \times Pr$ (properties evaluated at film temperature)
Re	Reynolds number: $Re = (V_0 D_w)/v$ (properties evaluated at film temperature)
T	temperature (°C)
T_S	wire surface temperature (°C)
T_∞	pool temperature (°C)
V	voltage (VDC)
V_0	velocity given by Eq. (18) (m/s)
x_0	distance over which the Nusselt number is averaged (m)

Greek symbols

α	thermal diffusivity (m^2/s)
β	coefficient of volumetric expansion (1/K)
ε	dielectric constant
ε_0	free space electric permittivity (F/m or C/V m)
μ	liquid dynamic viscosity (Pa·s)
v	kinematic viscosity (m^2/s)
ρ	liquid density (kg/m^3)
ρ_v	vapor density (kg/m^3)
σ_D	standard deviation of bubble departure diameters (m)

Subscripts

0	no electric field
Ratio	ratio of electric field quantity to no electric field quantity
FC	forced convection
LH	latent heat
NC	natural convection

due to variation in the dielectric constant, ε, with temperature. In single phase heat transfer, this force density term is affected by the thickness of the thermal boundary layer. Finally, the last term is referred to as dielectrophoresis, which represents the translational motion of neutral matter caused by polarization effects in a non-uniform electric field.

Numerous investigators have reported an increase in the boiling heat flux due to EHD [4–9]. Interest in EHD enhanced boiling was motivated by the fact that increased heat transfer rates can be obtained with minimal additional power consumption. However, the enhancement of fully developed nucleate boiling through the use of a high voltage electric field is limited. At high heat flux values where vigorous nucleate boiling exists, the extent of EHD enhancement has been relatively small (see, e.g. [8,10]).

One of the most pronounced effects of EHD on nucleate boiling is the reduction in the number of active nucleation sites due to increased convection, and hence, reduced surface temperature. The electric force acting on dielectric liquids augments convective heat transfer by applying an additional force on the fluid that aids the buoyancy force. At a given heat flux, an increase in the convective heat transfer coefficient results in a decrease in the temperature difference between the surface and the fluid, and hence the number of active nucleation sites. Many investigators have noted this reduction in the number of active nucleation sites including Bonjour et al. [11], Damianidis et al. [4], Kawahira et al. [5], and Yokoyama et al. [6].

An electric field also reduces the size of the departing vapor bubbles [12]. This effect was experimentally observed by Damianidis et al. [4], Baboi et al. [13], Allen

and Cooper [14], Karayiannis et al. [15], and Asch [16]. Because of the additional force acting on the bubbles, not only is the bubble departure size expected to be smaller, but also, the bubble growth period is expected to be shorter, i.e. the bubble departure frequency should be higher, as verified by Lovenguth and Hanesian [17].

Nucleate boiling hysteresis refers to the phenomenon where a given surface temperature superheat will result in two different heat fluxes depending on whether the heater surface is being heated or cooled. If the heater surface is being heated, a larger superheat is required to initiate nucleate boiling, while for a heater surface already experiencing boiling, a reduction in superheat will still produce large heat transfer rates. Application of an electric field tends to eliminate boiling hysteresis, with boiling incipience at a generally lower superheat [4,18,19].

The model of Paul and Abdel-Khalik [2] provides a systematic method for assessing the impact of EHD on bubble dynamics. The total heat flux in nucleate pool boiling is divided into three parts: (1) latent heat transfer, (2) forced convection, and (3) natural convection. The relative contributions of these mechanisms as the total heat flux is increased from boiling incipience to burnout can be quantified from measured values of the number of active nucleation sites, bubble departure diameters, and

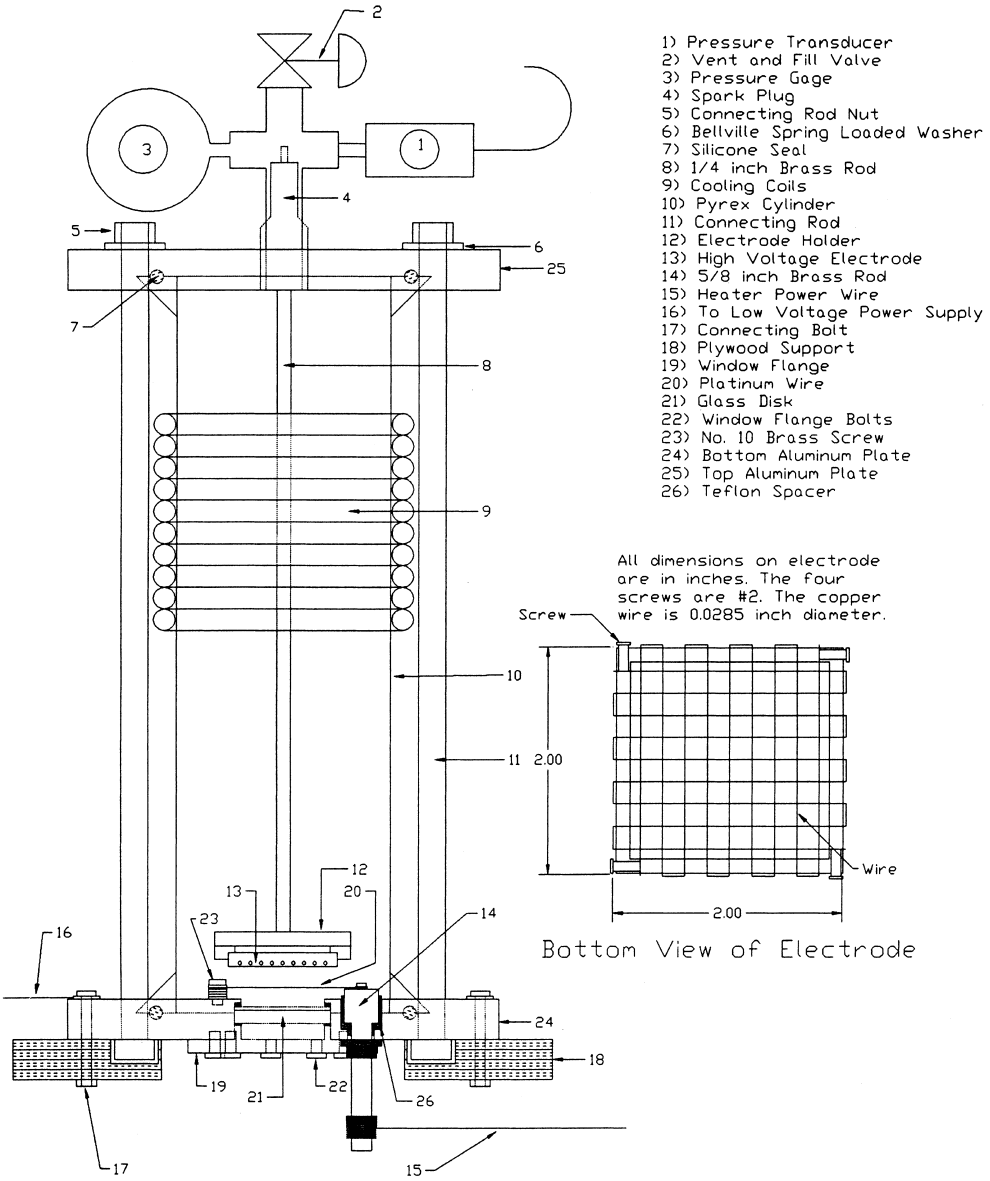

Fig. 1. Platinum wire experimental test facility.

bubble departure frequencies. The experiments conducted in this investigation allow measurement of these parameters with and without an electric field. Hence, the impact of EHD on the relative contributions of the above three mechanisms can be quantified.

2. Experimental apparatus

Saturated pool boiling of R-123 along an electrically heated horizontal platinum wire under the influence of a uniform electric field has been investigated. A schematic diagram of the experimental apparatus is shown in Fig. 1.

A platinum wire, 0.13 mm in diameter and 5.6 cm long, was used as the heat source. Fig. 2 shows the platinum wire attached to its power supply, as well as its current and voltage measuring devices. Since the resistance of the platinum changes linearly with temperature, the average heat flux and surface temperature can be calculated from the measured current and voltage drop. Prior to commencing the experiments, the wire was calibrated against a standard resistance thermometer (Omega Model ASL T100-250, Serial 440037). From the calibration results, a 0.6°C change in temperature results in a 0.001 Ω change in platinum wire resistance. A multimeter (HP3468A) was used to measure the current supplied to the wire, while an external bus data

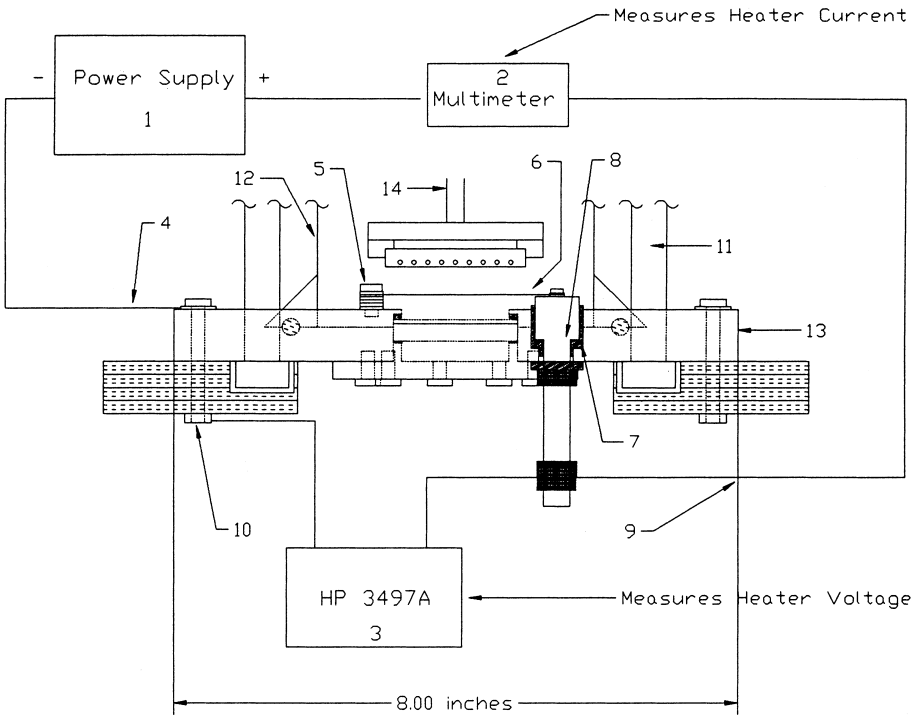

1) HP 6296A DC Power Supply, 0-60V, 0-3A
2) HP 3468A Multimeter
3) HP 3497A Data Acquisition/Control Unit
4) Heater Power Return Cable
5) No. 10 Brass Screw
6) Platinum Wire Heater
7) Teflon Spacer
8) Brass Rod
9) Heater Power Supply Cable
10) Connecting Bolt
11) Connecting Rod
12) Pyrex Cylinder
13) Aluminum End Plate (8 inch square)
14) High Voltage Square Electrode

Fig. 2. Platinum wire heater power supply system.

acquisition system (HP3497A Data Acquisition/control unit) was used to measure the voltage drop across the wire. Based on the manufacturers calibration, the multimeter was accurate to 0.14% of the reading for currents (<1 amp and 1% of the reading for currents >1 amp. Also, based on the manufacturers calibration, the data acquisition system was accurate to 0.002% of the voltage reading.

The housing of the experimental apparatus was made from a single 100 mm diameter, 30 cm long, Pyrex cylinder with grooves in both ends to accept o-ring seals. Aluminum plates were attached to both ends of the Pyrex cylinder to seal the cylinder from the atmosphere. The end plates also provided penetrations for connections to the interior of the system.

Three penetrations were made in the bottom aluminum plate. The first penetration was used to supply power to the platinum wire. The second penetration allowed for the placement of a calibrated thermocouple in the R-123 pool, while the third penetration accommodated a viewing window for imaging bubble dynamics under boiling conditions. The platinum wire was attached to the end of a 5/8 in. diameter brass rod, which was electrically isolated from the bottom aluminum plate using a Teflon spacer. A brass screw and brass washers attached the other end of the platinum wire to the bottom aluminum plate. In this manner, the bottom aluminum plate was used to complete the electrical circuit for the heater (Fig. 2).

The top aluminum plate contained two penetrations. The first penetration allowed for attachment of a pressure transducer, pressure gage, and a shut-off valve. The valve was used while evacuating and filling the system. The calibrated pressure transducer was used to verify the saturation conditions of R-123 inside the cylinder. The second penetration located in the center of the top plate was used for a modified automotive spark plug. The spark plug allowed for a reliable and inexpensive high voltage feedthrough. A brass rod, 1/4 in. diameter, was attached to the bottom of the spark plug. As seen in Figs. 1 and 2, a square wire mesh was attached to the bottom of this brass rod. The square mesh located 10 mm above the platinum wire was used to create the uniform electric field on the heater surface. A 0–30 kV high voltage power supply (Glassman Model PS/MJ30P0400-11) was used to supply voltage to the square mesh through the spark plug and brass rod. The platinum wire and the high voltage electrode were both submerged in the pool of liquid R-123, which was maintained at saturation conditions at a pressure of nearly 80 kPa.

At four different heat flux values with and without an applied electric field, bubble dynamics along the heated surface were imaged using a high-speed digital camera (Dalsa CA-D1-128D) operated at 770 frames/s. One hundred images at 12 locations along the wire were taken, i.e. a total of approximately 1200 images were obtained for each of the eight conditions. These images were individually viewed to determine the average number of active nucleation sites, the bubble departure diameters, and the bubble departure frequencies. A more detailed description of the apparatus and experimental procedure can be found in [20].

3. Experimental results

Bubble dynamics at four different heat flux values, viz. 7.5, 10.2, 12.4 and 14.5 W/cm^2, with and without an applied electric field of 10 kV potential were examined. The high-speed video images were used to determine the effect of the applied electric field on the contributions of various mechanisms to the total heat flux following the model of Paul and Abdel-Khalik [2]. In addition to these detailed bubble dynamics experiments, the effect of the electric field on the boiling curve over the heat flux range 0.9–14.5 W/cm^2 was determined. As expected, for a given heat flux, application of the electric field enhances natural convection, thereby suppressing boiling because of the lower heated surface temperature. Alternatively, for a given surface temperature, the presence of the electric field significantly increases the heat flux (Fig. 3).

The average surface heat flux was calculated from the measured current and voltage

$$q'' = \frac{VI}{\pi D_w L}. \tag{2}$$

The estimated average error in the surface heat flux was 2.2%; the major contributions to this error were the current measurement and uncertainty in the measured wire diameter.

The boiling curves shown in Fig. 3 cover the heat flux range from 0.9 to 14.5 W/cm^2, for both zero and 10 kV electrode voltage. To avoid boiling hysteresis during the

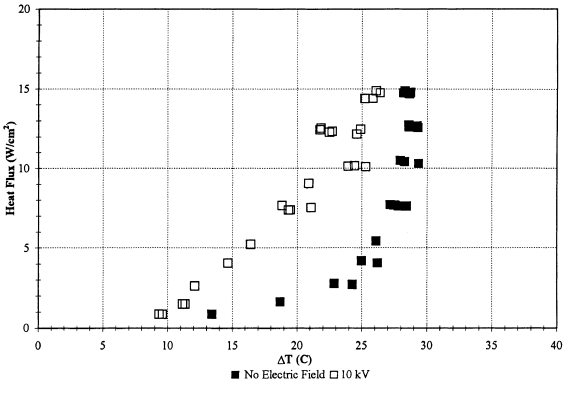

Fig. 3. Platinum wire experiments boiling curve with and without an electric field.

experiments, the heat flux was first raised above the desired value, and was then reduced to the desired level before data were collected. The surface temperature superheat is defined by

$$\Delta T \equiv T_S - T_\infty, \tag{3}$$

where T_S and T_∞ are the measured wire surface temperature and pool temperature, respectively. The saturation temperature calculated from the measured system pressure matched the directly measured pool temperature, thus verifying saturation conditions inside the cylinder. The error in ΔT was estimated to be 0.4°C for

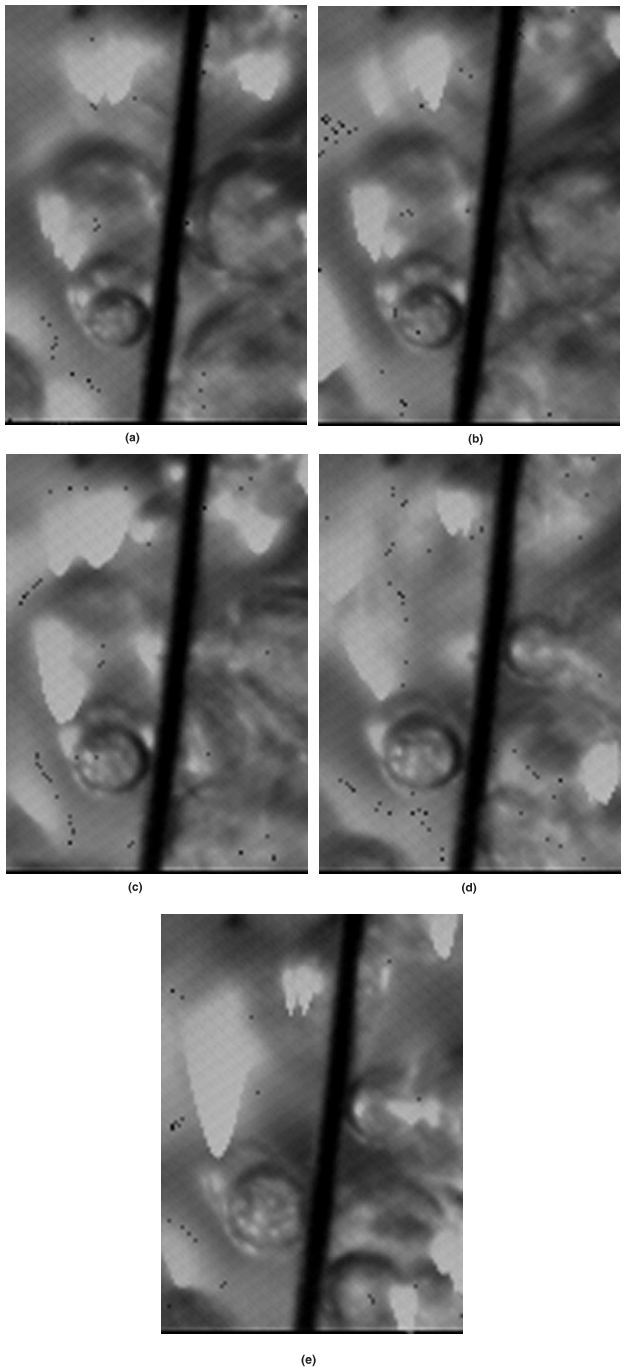

Fig. 4. Typical images from experiment at 12.4 W/cm^2 without an electric field.

heat fluxes less than 4 W/cm^2 and 3.0°C for heat fluxes greater than 4 W/cm^2.

Referring to Fig. 3, the zero voltage data covers the entire range from natural convection to nucleate boiling as evident by the large difference in the slope as ΔT is increased. With an applied electric field, the change in slope of the data was not as dramatic because of the significant enhancement in heat flux during natural convection. The enhancement was, clearly, more significant during natural convection than in the nucleate boiling regime. Nevertheless, the 10 kV data were higher than the 0 kV data over the entire surface temperature range. The enhancement of natural convection with an applied electric field was discussed in a previous article [21].

3.1. Bubble dynamics

The effect of EHD on bubble dynamics was experimentally examined using high-speed video at four different heat fluxes with and without an applied voltage. Each of the eight sets of data consisted of 1200 images with 100 images at 12 different positions along the wire, corresponding to a total imaged length of 3.1 cm of the 5.6 cm long wire. At each of the 12 locations along the wire, all the nucleation sites were counted. The nucleation sites were identified by viewing all 100 images at each of the 12 locations in a movie format. The estimated error in the average number of nucleation sites per unit length, $\langle N \rangle$, was 1.7%; the largest source of error was the uncertainty in the image magnification factor. Typical images from an experiment with no electric field at 12.4 W/cm^2 are shown in Fig. 4. In this figure, the dark line is the platinum wire. In this time sequence, a bubble is growing near the bottom of the image on the left side of the wire. This bubble departs the wire between the fourth and fifth images. Each image from (a) to (e) represents a time step of 0.0013 s.

For each of the 12 locations, the frame of each bubble departure was identified by viewing a movie of the entire 100-image sequence. The corresponding bubble departure diameters were measured using a magnified printed image of the identified frame. Based on the measurement and magnification factor errors, the estimated error in the bubble diameter measurement was 0.055 mm. For a given heat flux, all the bubble data at 12 locations were analyzed statistically. Figs. 5(a) and (b) show typical bubble departure diameter distributions without and with an electric field at 14.5 W/cm^2, respectively. The dashed line is a normal distribution, while the solid line is the asymptotic expansion of the normal frequency function. While there was a slight skewness and kurtosis with most of the bubble size distribution data, a normal distribution assumption introduced negligible error in the final analysis, and was, therefore, adopted.

The average bubble departure frequency, $\langle F \rangle$, was determined from the experimental data, by counting the

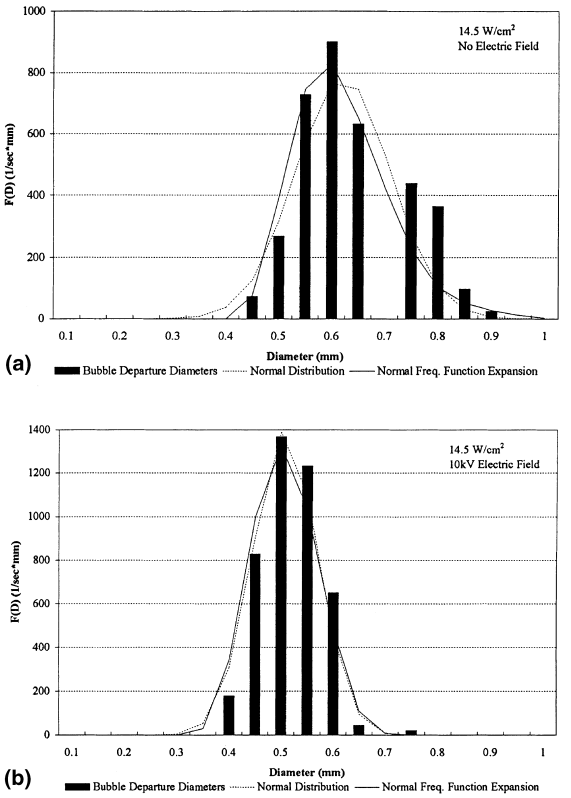

Fig. 5. (a) Typical bubble departure diameter distribution (without electric field). (b) Typical bubble departure diameter distribution (with electric field).

number of frames between consecutive bubble departures. The bubble period was calculated by dividing the number of frames by the frame rate (770 frames/s). At least 50 bubble departures were counted in order to obtain a statistically significant sample. The estimated error in the bubble departure period was 0.0013 s, which corresponds to the time between two consecutive frames.

The latent heat component, q''_{LH}, is calculated from the measured experimental quantities using the relation [2]

$$q''_{\mathrm{LH}} = \frac{1}{\pi D_{\mathrm{w}}} \langle N \rangle \langle J \rangle \langle F \rangle, \tag{4}$$

where $\langle N \rangle$ is the average number of nucleation sites per unit length, $\langle J \rangle$ the average heat removal per bubble, and $\langle F \rangle$ the average bubble departure frequency. For a normal distribution of bubble departure diameters, $\langle J \rangle$ is given by Paul and Abdel-Khalik [2]

$$\langle J \rangle = \frac{\pi}{6} \langle D \rangle^3 \rho_{\mathrm{v}} h_{\mathrm{fg}} \left[1 + \left(\frac{\sqrt{3}\sigma_{\mathrm{D}}}{\langle D \rangle} \right)^2 \right], \tag{5}$$

where $\langle D \rangle$ is the average bubble departure diameter. Error propagation analysis showed that the estimated error in the value of $\langle J \rangle$ was 28%, with the largest contributor being the error in bubble departure diameter. As a result, the estimated error in the calculated latent heat flux contribution, q''_{LH}, was 39%.

The above procedure was used to calculate q''_{LH} at the four different heat fluxes examined with and without an electric field. For a given heat flux, the ratio between the q''_{LH} values with and without an electric field was calculated

$$q''_{LH,Ratio} = \frac{q''_{LH}}{q''_{LH_0}}. \tag{6}$$

Values of $q''_{LH,Ratio}$ at the four different heat fluxes are plotted in Fig. 6(a). A zero value of $q''_{LH,Ratio}$ implies no latent heat flux contribution with an electric field, i.e. no active nucleation sites, which also implies a zero forced convection contribution, so that the entire heat transfer process is achieved by natural convection. A value of unity implies that the electric field has no impact on the latent heat contribution to the total heat flux.

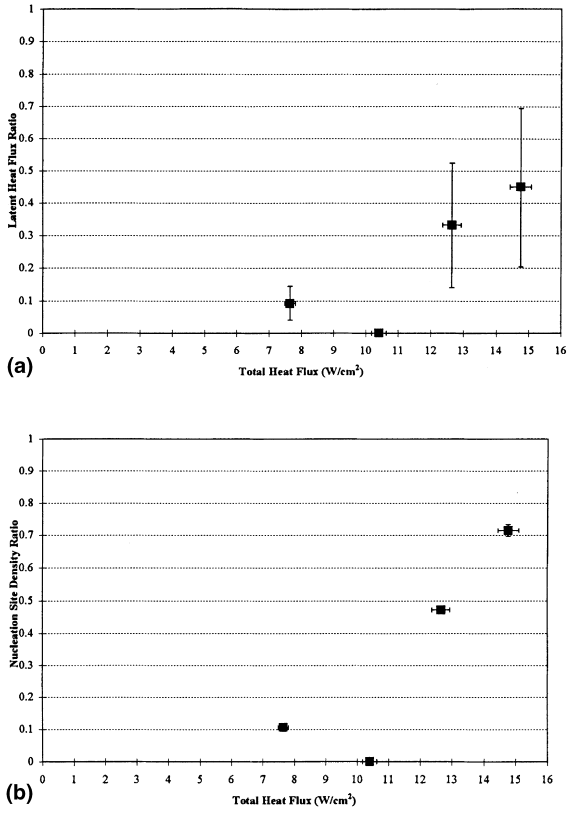

Fig. 6. (a) Ratio between latent heat flux components with and without an electric field. (b) Ratio between nucleation sites density values with and without an electric field.

Fig. 6(a) illustrates the dramatic effects of EHD on the boiling process, particularly at low heat fluxes. Referring to Fig. 6(a), at the two lowest heat flux values examined (7.5 and 10.2 W/cm^2), the latent heat flux contribution at an applied voltage of 10 kV was less than 10% of its value without an electric field. This means that the majority of heat transfer was achieved by natural convection, even though the surface temperature of the wire was actually reduced (see Fig. 3), which, in turn, reduced the number of active nucleation sites (Fig. 6(b)), and hence the latent heat and forced convection contributions to the total heat flux. The zero value of $q''_{LH,Ratio}$ at a heat flux of 10.2 W/cm^2 means that no active nucleation sites were observed at that heat flux when an electric field was applied. Fig. 6(a) also shows that at the two higher heat flux values examined (12.4 and 14.5 W/cm^2), the latent heat flux ratio is less than 50%. This, again, means that natural convection was enhanced, the surface temperature was reduced, and the number of active nucleation sites was also reduced (Fig. 6(b), albeit to a smaller extent than was the case at the lower heat flux values. The large uncertainty in the calculated values of $q''_{LH,Ratio}$, as displayed in Fig. 6(a), does not impact the above observations.

Fig. 6(b) shows variations of the ratio between the average number of nucleation sites per unit length with and without an applied voltage of 10 kV:

$$\langle N_{Ratio} \rangle = \frac{\langle N \rangle}{\langle N_0 \rangle}. \tag{7}$$

The data shown in Fig. 6(b) are consistent with the above observations regarding the effect of the applied electric field on natural convection, and hence the surface temperature, and the latent heat flux contribution (Fig. 6(a). The estimated error in the nucleation site density ratio was only 2.5%, with the largest contribution being the error in the image magnification factor.

The effect of the applied electric field on the average bubble departure diameters was quantified by plotting the ratio between the corresponding values with and without an electric field:

$$\langle D_{Ratio} \rangle = \frac{\langle D \rangle}{\langle D_0 \rangle}. \tag{8}$$

Fig. 7 shows variation of $\langle D_{Ratio} \rangle$ with the total heat flux; only three data points are shown since boiling was completely suppressed by the electric field at the second lowest heat flux value (see Figs. 6(a) and (b)). These results show that, as expected, the applied electric field reduces the average bubble departure diameter. Variations in $\langle D_{Ratio} \rangle$ over the examined heat flux range were within the estimated error of ± 0.11.

Figs. 6(a) and (b) and Fig. 7 clearly illustrate the effect of the applied electric field on the latent heat flux contribution, and by inference, on the natural convec-

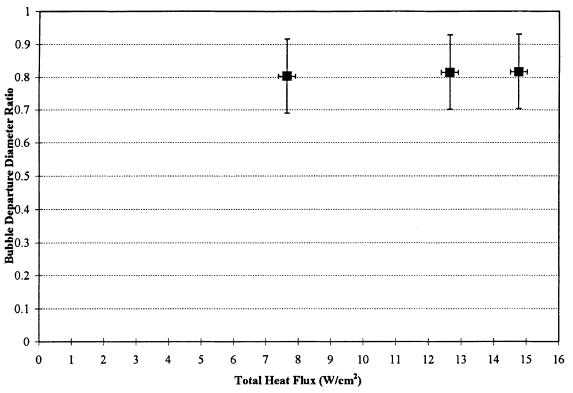

Fig. 7. Ratio between average bubble departure diameter values with and without an electric field.

tion contribution to the total heat flux. In order to assure internal consistency of the data, the natural convection and forced convection contributions to the total heat flux for the eight cases examined were directly calculated following the methodology presented by Paul and Abdel-Khalik [2]. Convection from that portion of the heated surface not occupied by bubbles accounts for the remainder of the heat flux. This convection is divided into two components: natural convection and forced convection. The natural convection component of the total heat flux, which accounts for 100% of the total heat flux prior to the onset of nucleate boiling, was calculated using the following equation:

$$q''_{NC} = \frac{k}{D_w} Nu_{NC} (T_S - T_\infty) f_{NC}, \tag{9}$$

where f_{NC} is the fraction of the heated surface experiencing natural convection. The Nusselt number in the low Rayleigh number range of the experiments was calculated using a correlation developed in [2] based on the data of McAdams [22]

$$Nu_{NC} = (1.000) Ra^n \quad (Ra \leqslant 10^4), \tag{10}$$

where the exponent n is given by

$$n = 0.130 + 0.0125 \log(Ra). \tag{11}$$

The natural convection component of the total heat flux, Eq. (9), in the EHD-enhanced experiments was modified as follows

$$q''_{NC} = \frac{k}{D_w} (Nu_{NC} + \Delta Nu_{NC})(T_S - T_\infty) f_{NC}, \tag{12}$$

where ΔNu_{NC} represents the enhancement in the Nusselt number over the natural convection value caused by the electric field. The natural convection Nusselt number, Nu_{NC}, was calculated using Eqs. (10) and (11), while ΔNu_{NC} was calculated using the empirical correlation of Pascual et al. [21]

$$\Delta Nu_{NC} = 0.0895 Ra_{El}^{0.365}. \tag{13}$$

Here, the electric Rayleigh number, Ra_{El}, is given by:

$$Ra_{El} = El \times Pr. \tag{14}$$

The electrical number, El, is defined by [20,21]

$$El = \frac{\rho(d\varepsilon/dT) D_w^2 \Delta T \varepsilon_0 E^2}{\mu^2}. \tag{15}$$

The transport properties of liquid R-123 were obtained from the ASHRAE Handbook [23], while the dielectric constant and its dependence on temperature were found in Tanaka et al. [24]. The electric field strength at the heat transfer surface, E, was calculated from a numerical solution of Laplaces equation, as described in Pascual [20]. The temperature difference between the heated surface and the pool corresponds to the measured experimental values. The estimated error in the ΔNu_{NC} value was 21%, primarily due to uncertainties in the measured temperature difference and wire diameter.

Bubble growth and departure on the heated surface cause agitation of the thermal boundary layer in the vicinity of the nucleation sites. The contribution of this effect, referred to as forced convection, can be estimated using the relation [2]

$$q''_{FC} = \frac{k}{D_w} Nu_{FC} (T_S - T_\infty) f_{FC}, \tag{16}$$

where f_{FC} is the fraction of the surface experiencing forced convection. For experiments without an applied electric field, the Nusselt number in Eq. (16) was estimated using a forced convection correlation for flow across a heated cylinder developed by Hilpert [25]

$$Nu_{FC} = C_1 Re_{D_w}^{C_2}. \tag{17}$$

Values for $C_1$and C_2 are given in Table 1.

The characteristic velocity in the Reynolds number used in the above correlation was calculated using the relation [2]

$$V_0 = \langle D \rangle \langle F \rangle. \tag{18}$$

The surface fractions experiencing each of the three heat transfer modes discussed above, f_{LH}, f_{NC}, and f_{FC}, were estimated as follows:

Table 1
Constants for circular cylinder Nusselt number in cross flow (Eq. (17))

Re_D	C_1	C_2
1–4	0.891	0.330
4–40	0.821	0.385
40–4000	0.615	0.466
4000–40,000	0.174	0.618
40,000–250,000	0.024	0.805

$$f_{LH} = f_g \langle D \rangle \langle N \rangle, \tag{19}$$

where f_g is the average fractional chord length of a spherical bubble in contact with the heated surface, as estimated from the experimental images. The forced convection fraction is estimated from the influence distance near an active nucleation site that is affected by the bubble, $f_1\langle D \rangle$, so that

$$f_{FC} = 2 f_1 \langle D \rangle \langle N \rangle. \tag{20}$$

The surface fraction experiencing natural convection, f_{NC}, is calculated using the relation

$$f_{NC} = 1 - f_{LH} - f_{FC}. \tag{21}$$

From the bubble images, the value of f_g was estimated to be 0.34 with no applied electric field and 0.32 with a 10 kV electric potential. The value of f_{LH} was then calculated using Eq. (19). The value of f_1 was estimated to be 0.45, so that the fraction of the surface experiencing forced convection was

$$f_{FC} = 2(0.45)\langle D \rangle \langle N \rangle. \tag{22}$$

Eq. (21) was then used to calculate the value of f_{NC}.

The estimated error in the f_{NC} values was 0.27 for the no electric field experiments and 0.12 for the 10 kV electric potential experiments. The largest contribution to this uncertainty was the error in the imaged wire length (i.e. magnification factor), along with the error in the bubble diameter. The smaller error in f_{NC} when an electric field is applied is due to the fact that a smaller fraction of the surface was involved in either latent heat transport or enhanced convection. The resulting error in the natural convection heat flux component, q''_{NC}, was estimated to be 2.0 W/cm^2 for experiments with the applied electric field and 1.0 W/cm^2 for experiments without an electric field. The largest contribution to this uncertainty was the error in f_{NC}, which accounts for nearly 60% of the error in q''_{NC}.

Values of q''_{NC} for the eight experiments examined are plotted in Fig. 8(a). These results clearly illustrate the significant enhancement in q''_{NC} due to the applied electric field over the entire range of heat flux values examined. The data also illustrate that at the highest heat flux where the natural convection contribution without EHD was essentially zero, the natural convection component remains significant when an electric field is applied.

In order to calculate the forced convection contribution to the total heat flux, Eq. (17) was used to determine the forced convection Nusselt number for cases without an applied electric field. Because of the transient nature of the bubble cycle and since a distribution of velocities was obtained for each experiment, an average Nusselt number was calculated [2]

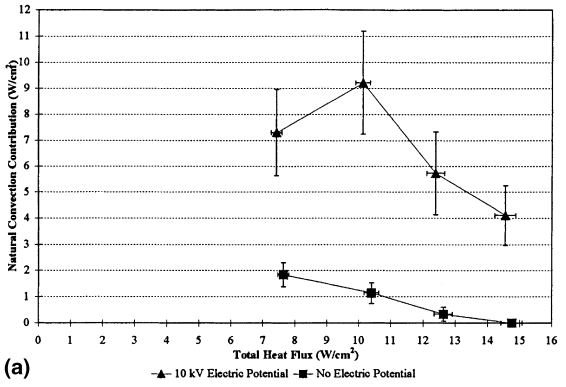

Fig. 8. (a) Variation of natural convection contribution to the total heat flux with and without an electric field. (b) Variation of forced convection contribution to the total heat flux with and without an electric field.

$$\langle Nu_{FC} \rangle = \frac{Nu_0}{\left(\dfrac{x_0}{f_1\langle D \rangle}\right)(1+C_2)} \left[1 - \left(1 - \frac{x_0}{f_1\langle D \rangle}\right)^{1+C_2}\right], \tag{23}$$

where Nu_0 was calculated using Eq. (17) with the Reynolds number calculated using V_0 from Eq. (18). The distance x_0 was either $f_1\langle D \rangle$ or one-half the average distance between bubbles, whichever was smaller. For the platinum wire experiments, $f_1\langle D \rangle$ was always smaller than one-half the average distance between the bubbles; therefore, the average Nusselt number simplified to

$$\langle Nu_{FC} \rangle = \frac{Nu_0}{1+C_2}. \tag{24}$$

For experiments with an applied electric field, the forced convection heat flux, Eq. (16), was modified to account for the electric field enhancement as follows:

$$q''_{FC} = \frac{k}{D_w}(\langle Nu_{FC} \rangle + \Delta Nu)(T_S - T_\infty) f_{FC}, \tag{25}$$

where ΔNu represents the enhancement in the single phase Nusselt number due to the presence of the electric field, which was estimated using Eq. (13). This approach was justified by the fact that the ratio $El/Re_{D_w}^2 \approx 1$ so that the effect of electric field enhancement on the forced convection heat transfer coefficient could not be ignored.

The estimated error in the Nusselt number was 16% and 12% for experiments with and without an electric field, respectively, while the estimated error in f_{FC} was 10%. The corresponding estimated error in the forced convection heat flux, q''_{FC}, was 20% and 14% for experiments with and without an electric field, respectively; the largest contributions to this uncertainty were the errors in Nu, ΔT, and f_{FC}.

Values of q''_{FC} for the eight experiments examined are plotted in Fig. 8(b). These results are clearly consistent with those presented in Figs. 6(a) and 8(a) for the latent heat flux ratio and natural convection contribution. At low heat fluxes, the electric field enhances natural convection and suppresses boiling by reducing the number of active nucleation sites, thereby reducing the forced convection contribution to the total heat flux.

Fig. 9(a) and (b) show the combined effect of natural convection, latent heat transfer, and forced convection as a function of total heat flux without and with an applied electric field, respectively. Fig. 9(a) shows that, for the case without an electric field, as the total heat flux increases, the natural convection contribution becomes insignificant and vanishes at nearly 14.5 W/cm^2. At that point, the contributions to the total heat flux by latent heat transport and forced convection are nearly equal. At higher heat fluxes, the latent heat contribution is expected to increase approaching 100% of the total heat flux as CHF is approached. The error shown in Fig. 9(a) was calculated based on the difference from 100% between the experimental total heat flux and the sum of the apriori calculations of the three components contributing to the total heat flux.

Fig. 9(b) shows the fractional contribution to the total heat flux of the three forms of heat transfer with an applied 10 kV electric potential. While the overall trends for the relative contributions of the three components are the same as those for the case without an electric field (Fig. 9(a)), it is clear that natural convection continues to significantly contribute to the total heat flux at significantly elevated heat flux values. At 14.5 W/cm^2, natural convection accounted for almost 30% of the total heat transfer, versus zero for the case without an electric field. The latent heat and forced convection contributions were insignificant below 10.2 W/cm^2. These results are clearly consistent with those presented earlier for the impact of the electric field on the individual components. While the data in Figs. 9(a) and (b) does not extend to heat flux values approaching CHF, one may infer from Fig. 9(b) that the presence of the electric field should increase the value of CHF. Again

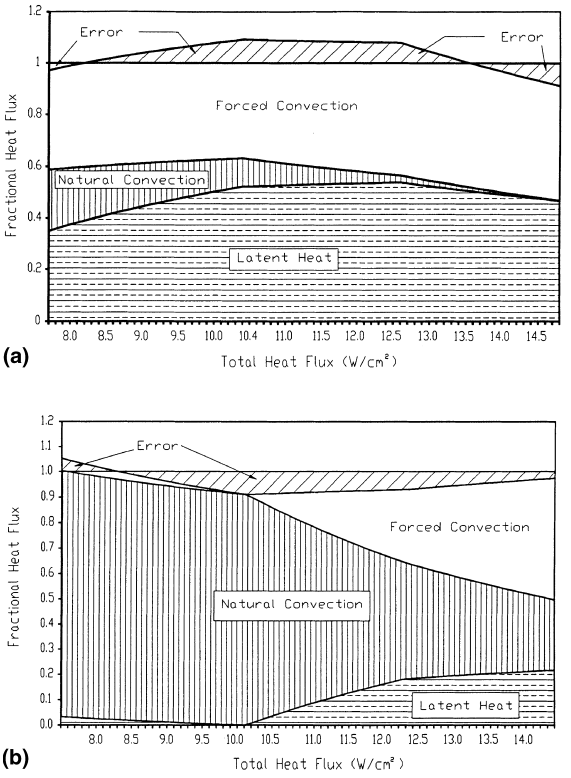

Fig. 9. (a) Relative heat flux contributions for experiments with no electric field. (b) Relative heat flux contributions for experiments with 10 kV electric potential.

the error in Fig. 9(b) was calculated based on the difference from 100% between the experimental heat flux and the sum of the a priori calculations of the three components contributing to the total heat flux.

3.2. Concluding remarks

The primary purpose of this investigation was to quantify the effect of electric forces on bubble dynamics in nucleate pool boiling. High-speed video images were obtained for saturated pool boiling along a thin platinum wire immersed in HCFC-123, with and without an applied uniform electric field. The effect of the electric field on the boiling curve was quantified. Additionally, the bubble dynamics data were used to determine the effect of the applied electric field on the contributions of natural convection, forced convection, and latent heat removal to the total heat flux over a wide range of heat flux values.

The data show that for a given heat flux, the presence of the electric field significantly increases the natural convection contribution to the total heat flux over an extended range of heat flux values. Additionally, the presence of the electric field reduces the contribution of

latent heat transport to the total heat flux, primarily, due to the reduction in the number of active nucleation sites. The data also show that the presence of the electric field reduces the average bubble departure diameter, with little variation of the extent of reduction over the examined heat flux range. The reduction in latent heat transport at low heat fluxes produces a commensurate reduction in the forced convection contribution to the total heat flux.

The data obtained in this investigation provide the means to validate future mechanistic models for the effect of EHD on boiling heat transfer.

References

[1] L.W. Chubb, Improvements relating to methods and apparatus for heating liquids, UK Patent No. 100, 796, 1916.

[2] D.D. Paul, S.I. Abdel-Khalik, A statistical analysis of saturated nucleate boiling along a heated wire, Int. J. Heat Mass Transfer 26 (1983) 509–519.

[3] J.A. Stratton, Electromagnetic Theory, McGraw-Hill, New York, 1941.

[4] C. Damianidis, T.G. Karayiannis, R.K. Al-Dadah, R.W. James, M.W. Collins, P.H.G. Allen, EHD boiling enhancement in shell-and-tube evaporators and its application in refrigeration plants, ASHRAE Transactions: Symposia BA-92-5-5, 1992, pp. 462–472.

[5] H. Kawahira, Y. Kubo, T. Yokoyama, J. Ogata, The effect of an electric field on boiling heat transfer of refrigerant-11 – boiling on a single tube, IEEE Trans. Industry Appl. 26 (2) (1990) 359–365.

[6] T. Yokoyama, T. Yamazaki, Y. Kubo, J. Ogata, A. Kawada, Y. Ooki, The effect of an electric field on boiling heat transfer of fluorocarbon R-11, in: Proceedings of the XVIII International Centre for Heat and Mass Transfer, Dubrobnik, Yugoslavia, 1986, pp. 140–151.

[7] R.A. Blachowicz, Boiling heat transfer in an electrical field, Chem. Engrg. Sci. 35 (1980) 761–762.

[8] K.H. Cheung, M.M. Ohadi, S. Dessiatoun, Compound enhancement of boiling heat transfer of R-134a in a tube bundle, ASHRAE Transactions: Symposia CH-95-14-1, 1995, pp. 1009–1019.

[9] R.K. Al-Dadah, T.G. Karayiannis, P.H.G. Allen, Electrohydrodynamic heat transfer enhancement in flooded evaporators, Thermodynamics and the Design, Analysis, and Improvement of Energy Systems, AES-Vol. 33, ASME, 1994, pp. 41–56.

[10] M.M. Ohadi, R.A. Papar, T.L. Ng, M.A. Faani, R. Radermacher, EHD enhancement of shell-side boiling heat transfer coefficients of R-123/Oil Mixture, ASHRAE Transactions, 98 (2) (1992) 427–434.

[11] E. Bonjour, J. Verdier, L. Weil, Electroconvection effects on heat transfer, Chem. Engrg. Prog. 58 (1962) 63–66.

[12] J. R. Melcher, in: Field Coupled Surface Waves: A Comparative Study of Surface-coupled Electrodynamic and Magnetohydrodynamic Systems, MIT Press, Cambridge, MA, 1963, pp. 27–76.

[13] N.F. Baboi, M.K. Bologa, A.A. Klyukanov, Some features of ebullition in an electric field, Appl. Elecr. Phenom., USSR 20 (1968) 57–70.

[14] P.H.G. Allen, P. Cooper, The potential of electrically enhanced evaporators, in: Proceedings of the Third International Symposium on the Large Scale Application of Heat Pumps, Oxford, UK, 1987, pp. 221–229.

[15] T.G. Karayiannis, M.W. Collins, P.H.G. Allen, Electrohydrodynamic enhancement of nucleate boiling heat transfer in heat exchangers, J. Chem. Engrg. Commun. 81 (1989) 15–24.

[16] V. Asch, Electrokinetic phenomena in boiling freon-113, J. Appl. Phys. 37 (7) (1966) 2654–2658.

[17] R.F. Lovenguth, D. Hanesian, Boiling heat transfer in the presence of non-uniform direct current electric fields, Ind. Engrg. Chem. Fundam. 10 (1971) 570–576.

[18] D.K. Basu, Effect of electric field on boiling hysteresis in carbon tetrachloride, Int. J. Heat Mass Transfer 16 (1973) 1322–1324.

[19] J.H. Stromberger, An experimental investigation of electrohydrodynamic (EHD) enhancement of boiling heat transfer, Masters thesis, Georgia Institute of Technology, Atlanta, GA, 1997.

[20] C.C. Pascual, Electrohydrodynamic enhancement of nucleate pool boiling, Ph.D. thesis, Georgia Institute of Technology, Atlanta, GA, 1999.

[21] C.C. Pascual, J.H. Stromberger, S.M. Jeter, S.I. Abdel-Khalik, An empirical correlation for electrohydrodynamic enhancement of natural convection, Int. J. Heat Mass Transfer 43 (11) (2000) 1965–1974.

[22] W.H. McAdams, Heat Transmission, McGraw-Hill, New York, 1954, pp. 172–176.

[23] ASHRAE, ASHRAE Handbook Fundamentals, American Society of Heating, Refrigerating and Air-Conditioning Engineers, Atlanta, GA, 1993, pp. 17–23.

[24] Y. Tanaka, T. Tsujimoto, S. Matsuo, T. Makita, Dielectric constant of environmentally acceptable refrigerants HFC-134a, HCFC-123, and HCFC-141b under high pressures, Fluid Phase Equilibria 80 (1992) 107–117.

[25] R. Hilpert, Forsch. Geb. Ing. Wes. 4 (1933) 215.